ELSEVIER

Journal of Alloys and Compounds 317–318 (2001) 98–102

Journal of ALLOYS AND COMPOUNDS

www.elsevier.com/locate/jallcom

# Characterization of $RuO_2$ and $IrO_2$ films deposited on Si substrate

P.C. Liao[a,*], Y.S. Huang[b], K.K. Tiong[c]

[a]*Department of Electronic Engineering, Kung Wu Institute of Technology and Commerce, Peitou, Taipei 112, Taiwan, Republic of China*
[b]*Department of Electronic Engineering, National Taiwan University of Science and Technology, Taipei 106, Taiwan, Republic of China*
[c]*Department of Electrical Engineering, National Taiwan Ocean University, Keelung 202, Taiwan, Republic of China*

**Abstract**

$RuO_2$ and $IrO_2$ films, deposited on Si substrates by metal–organic chemical vapor deposition (MOCVD) method and reactive sputtering method under various conditions, were characterized by atomic force microscopy (AFM), X-ray diffraction, electrical conductivity, ellipsometry and Raman scattering measurements. The average grain sizes of the films were estimated by AFM. A grain boundary scattering model was used to fit the relation between the average grain size and electrical resistivity. The optical and dielectric constants were determined by the ellipsometry measurements. The results of the electrical and optical studies show a metallic character of the films deposited at higher temperatures. The red shift and broadening of the line width of the Raman peaks were analyzed and discussed. 

*Keywords:* Transition-metal dioxide; Electrical property; Optical property; Raman scattering

## 1. Introduction

$RuO_2$ and $IrO_2$ belong to the family of transition-metal dioxide compounds with rutile-type structure, which exhibit interesting properties such as low resistivity, high chemical and thermodynamic stability. $RuO_2$ and $IrO_2$ are well known as corrosion-resistant low overpotential electrodes for chlorine and oxygen evolution [1,2]. In recent research, $RuO_2$ films have shown great promise in various applications: in very large-scale integration (VLSI) [3,4], as a thick film resistor [5,6] or as a buffer layer for YBCO superconducting thin film (for reducing inter-diffusion and for improvement of proper phase) [7]. Furthermore, $RuO_2$ exhibits excellent diffusion barrier properties [8,9]. There is a great interest in $IrO_2$ for use as electrochromic displays [10], pH sensors [11], electrodes for neural stimulation [12] and high rate-high charge capacitors [13]. Although a considerable amount of applied research has been performed on $RuO_2$ and $IrO_2$, only relatively few experimental information on the properties of $RuO_2$ and $IrO_2$ films has been reported.

In this article we report a detailed characterization of the solid-state properties of $RuO_2$ and $IrO_2$ films deposited on Si substrates by metal–organic chemical vapor deposition (MOCVD) and reactive sputtering under different conditions. The morphology, structure and composition of the films are examined. The electrical conductivity measurements are carried out. The optical constants of $RuO_2$ and $IrO_2$ films are determined using spectroscopic ellipsometry. Finally, $RuO_2$ and $IrO_2$ films are characterized by Raman spectroscopy.

## 2. Experimental

### 2.1. Deposition of the $RuO_2$ and $IrO_2$ films

$RuO_2$ and $IrO_2$ films were deposited by using a hot-wall, laminar flow chemical vapor deposition (CVD) reactor. The reactor itself is a quartz tube with an inner diameter of 6.2 cm mounted horizontally inside a two-zone furnace. The reactor was evacuated to a pressure lower than $1 \cdot 10^{-3}$ Torr (1 Torr=133.322 Pa). The reaction gas $O_2$ was introduced into the reactor using independently controlled fine needle valves with $O_2$ maintained at a pressure of 0.8 atm and at a gas flow-rate of 200 $cm^3$/min (1 atm=101 325 Pa). To avoid turbulence of the reaction gas, substrates were laid on a quartz-plate layer in the reactor. All surfaces of the apparatus outside the reaction zone were maintained at temperatures greater than the precursor sublimation temperatures but lower than its decomposition temperatures so as to prevent condensation of the sublimable $Ru(C_5H_5)_2$ [or $Ir(C_5H_4CH_3)$(1,5-

*Corresponding author.
*E-mail address:* pcliao@msl.tisnet.net.tw (P.C. Liao).

0925-8388/01/$ – see front matter 
PII: S0925-8388(00)01403-1

$C_8H_{12}$)]. The vapor pressures at 85°C are about 0.01 Torr for $Ru(C_5H_5)_2$ and 0.005 Torr for $Ir(C_5H_4CH_3)(1,5\text{-}C_8H_{12})$. Gas flow through the reactor was laminar and parallel to the deposition surface. The axial temperature profile was measured before each experiment by positioning a thermocouple at various locations along the reactor axis. The deposition temperatures were in the range 600–500°C for $RuO_2$ and 450–350°C for $IrO_2$. The growth rates for $RuO_2$ and $IrO_2$ were about 10 nm/min and 5 nm/min, respectively.

$RuO_2$ and $IrO_2$ films with thicknesses in the range of 2500–3500 Å were also deposited in a custom-built reactive radio frequency (RF) magnetron sputtering system equipped with a rotary mechanical and turbo pumps. The target was a 1 in. diameter Ru (or Ir) sample with a purity of 99.99% before the deposition and was presputtered in $10^{-3}$ mbar of high-purity Ar gas for a few minutes (1 in.=2.54 cm). The sputtering chamber was evacuated to a pressure lower than $5\cdot10^{-5}$ mbar. The films were deposited on Si substrates. The substrate temperature during sputtering was kept in the range of 25–450°C. The reaction gases $O_2$ and Ar were introduced into the sputtering chamber using independently controlled fine needle valves with $O_2$ maintained at a pressure of $3\cdot10^{-3}$ mbar and the total working gas pressure ($Ar+O_2$) kept at a constant level of about $7.5\cdot10^{-3}$ mbar. The distance between substrate and target was fixed at 4 cm. The actual deposition time for the samples was about 3 min, and the sputtering rate was about 800–1200 Å/min for a sputtering power of 100 W.

### *2.2. Characterization of the films*

A Digital Instruments Nano-Scope III atomic force microscopy (AFM) instrument was employed to determine the average grain size and a Dektak 3030 profilemeter was used to observe the morphology and the thickness of the films. Characterization of the crystallinity of the films was performed using X-ray diffraction. Electrical resistivity measurements over the temperature range 4.2–300 K were made on films by the ordinary van der Pauw method using a Keithley 182 nanovoltmeter and a Keithley 220 constant current source. The residual resistivity ratio (RRR), defined as $\rho(300\ K)/\rho(4.2\ K)$, provides information on the electron mean free path, and thus will serve as an indicator for the average grain size. The RRR information of all the films correlating to the thickness, the substrate temperature, and the sputtering power were calculated.

The optical properties of the $RuO_2$ and $IrO_2$ films were studied by using ellipsometry. Variable-angle spectroscopic ellipsometry (VASE) measurements were taken in the spectral range from 0.8 to 5.0 eV at three different incident angles (65°, 70° and 75°). The details for the VASE method can be found in the literature [14]. Raman measurements in the back scattering geometry utilizing a Renishaw Raman Microscope system 2000 at room temperature were also performed. The resolution of the system was about 4 $cm^{-1}$. Spectra were taken with the 6328 Å excitation line of a He–Ne laser with a typical laser power of about 30 mW. The optical penetration depth of the laser light was about 40 nm for $RuO_2$ and $IrO_2$. To minimize heating, the laser intensity was reduced to about 10–30% of its initial value by using a neutral density filter and also the samples were mounted using thermal conductive grease on aluminum plates. A charge couple device (CCD) camera was used to pick up the scattered signals. The Raman spectra of the $RuO_2$ and $IrO_2$ films were obtained and compared with that of single crystals $RuO_2$ and $IrO_2$.

## 3. Results and discussion

Fig. 1 shows the AFM images of $RuO_2$ or $IrO_2$ films deposited at two representative substrate temperatures, with roughness estimated to be around 10–20 nm. The average grain size of $RuO_2$ films as a function of deposition temperature is also plotted in Fig. 2a, which shows a size variation from 12±3 to 50±5 nm in the temperature range considered. The average grain size for $IrO_2$ as a function of deposition temperature is also plotted in Fig. 2b. Our work showed evidence of increasing average grain

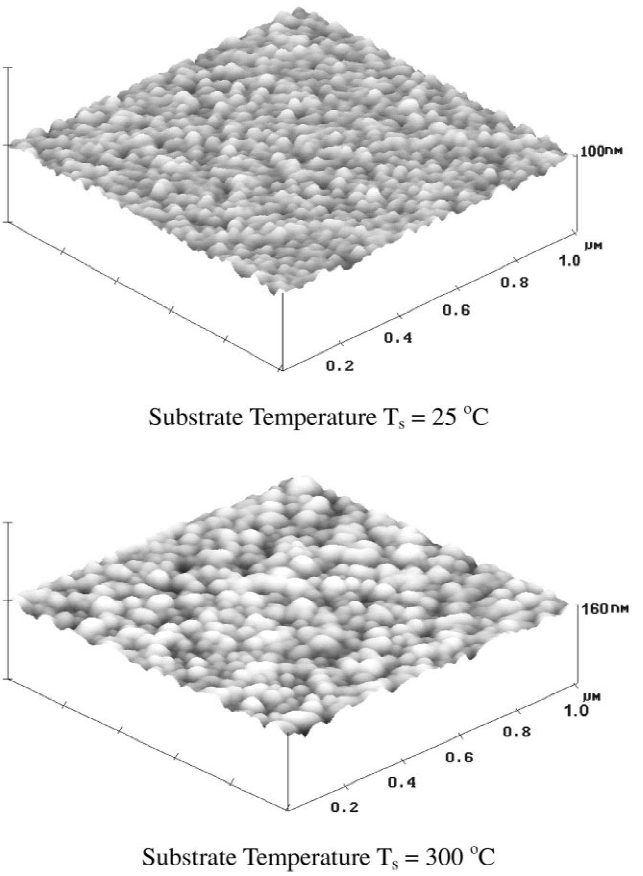


Fig. 1. The AFM images of $RuO_2$ films deposited at a substrate temperature of 300°C.

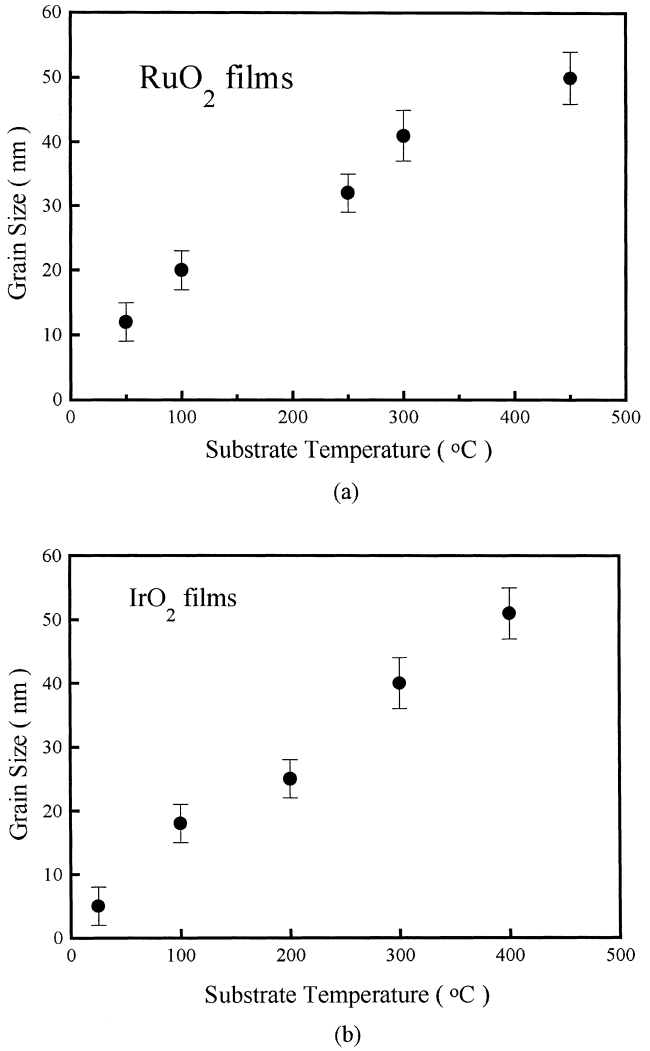


Fig. 2. (a) The average grain size of $RuO_2$ films as a function of substrate temperature. (b) The average grain size of $IrO_2$ films as a function of substrate temperature.

size with increasing substrate temperature from 25 to 400°C.

X-Ray diffraction measurements were also carried out to study the structure of $RuO_2$ and $IrO_2$ films. The results of the X-ray diffraction study indicate that there is no evidence of order for films deposited at substrate temperatures below 100°C. Order begins to appear upon heating the substrate above 100°C. In most cases, the basic rutile crystal structure of $RuO_2$ and $IrO_2$ is retained for a substrate temperature higher than 100°C. However, the diffraction peaks are increasingly shifted to smaller angles and the line width of the peaks increasingly broadened as the substrate temperature is decreased. The shift to lower angles and the increase of the broadening of diffraction peaks is attributed to microcrystallinity and local disorder. Auger electron spectroscopy was used to examine the composition of the as-deposited films. Our results show a slight oxygen deficiency with the actual composition to be about 1:1.99 and 1:1.98 for $RuO_2$ and $IrO_2$ films, respectively.

The van der Pauw method was used to measure the resistivity of the films as a function of temperature in the range 4.2–300 K. The room temperature resistivities of $RuO_2$ films are in the range 60 μΩ·cm–430 μΩ·cm and $IrO_2$ films are in the range 70 μΩ·cm–730 μΩ·cm. From the temperature dependent resistivity measurement, the RRR of the films can be evaluated. The RRR serves as an indicator of electron mean free path and hence provides information for the grain size of the $RuO_2$ and $IrO_2$ films. The RRRs for the as-deposited films are displayed in Fig. 3a and showed a general trend of increasing grain size with

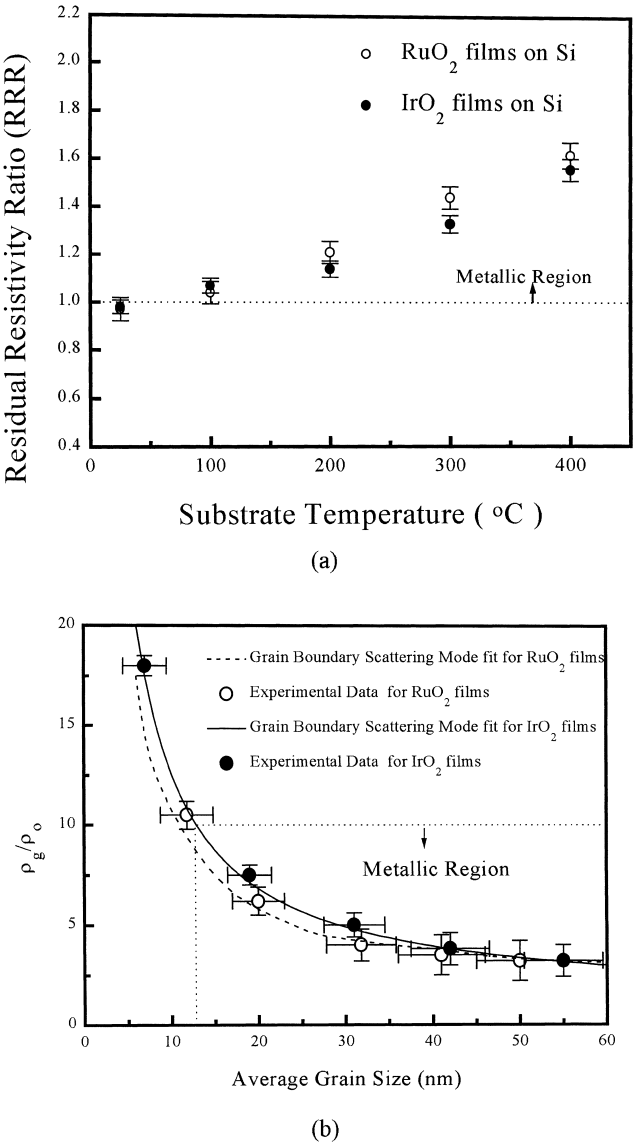


Fig. 3. (a) The residual resistivity ratios (RRRs) of the $RuO_2$ and $IrO_2$ films as a function of substrate temperature. (b) Fit of experimental data to the grain boundary scattering model with scattering coefficient $S=0.785$ and $S=0.812$ for $RuO_2$ and $IrO_2$, respectively, and electron mean free path $l_o=20$ nm, where $\rho_g$ and $\rho_o$ are, respectively, the grain boundary and bulk resistivities at 300 K.

substrate temperature. The different electrical behavior is clearly divided by the RRR=1 line, below which the deposited films lose their metallic character. For both films, the RRR=1 line occurred at substrate temperature around 100°C. The experimental data are fitted with the grain boundary scattering model described by Mayadas and Shatzkes, which is given as [15]:

$$\frac{\rho_g}{\rho_o} = \left[1 - \frac{3}{2}\alpha + 3\alpha^2 - 3\alpha^3 \ln\left(1 + \frac{1}{\alpha}\right)\right]^{-1} \quad (1)$$

where $\alpha = (l_0/d)\cdot(S/1-S)$, $\rho_g$ and $\rho_o$ are, respectively, the grain boundary and bulk resistivities at 300 K, $l_o$ is the mean free path, $d$ is the average grain size and $S$ is the grain boundary scattering coefficient. The model assumed columnar structure and this is precisely the morphology of the as-grown films in this study. The higher the $S$ value, the more significant the grain boundary effect in the scattering mechanism. As $S$ approaches unity, the resistivity of the films becomes infinite. At high $S$ values, the crystallinity of the films would play an increasingly important role in determining the electrical conductivity of the films. We used a typical mean free path of 20 nm in Eq. (1) to fit our experimental data. The results of our samples with grain sizes of 12–50 nm for $RuO_2$ and 7–55 nm for $IrO_2$ films agreed quite well with the theoretical prediction and are plotted in Fig. 3b. From the fit, the values of $S=0.785$ and $S=0.812$ are derived for $RuO_2$ and $IrO_2$, respectively. These values are much higher than that of 0.24 for Cu and 0.17 for Al. This means the dominant factor for the total resistivity in $RuO_2$ and $IrO_2$ microcrystalline films come from electron scattering due to grain boundary. Such a high value of the grain boundary scattering coefficient suggests useful application for the fabrication of metallic films with a wide range of resistivities.

The optical constants of the as-deposited films at room temperature were deduced from VASE measurements in the energy range 0.8–5 eV. The measured values of refractive index, $n$ and extinction coefficient, $k$ can be utilized to evaluate the real and imaginary parts of the dielectric constants for the films. These are illustrated in Fig. 4a and b for $IrO_2$ films. The optical properties of the materials in the visible or ultraviolet region are determined by the interband transitions, whereas in the IR region, the intraband transitions are dominant. For a free electron gas in the absence of any interband transitions, the real part of the dielectric constant $[\epsilon_1 = 1-(\omega_p^2/\omega^2)]$ becomes zero at the plasma frequency given by $\omega_p = (4\pi Ne^2/m^*)^{1/2}$, where $N$ is the density of free electrons, $e$ is the electronic charge, and $m^*$ is the effective mass of the electron inside the metal. However, in the presence of interband transitions, $\epsilon_1$ has both free and bound contributions and, starting from negative values, becomes zero at a frequency $\omega_{th} < \omega_p$ where $E_{th} \equiv \hbar\omega_{th}$ is the threshold energy for interband transitions. From Fig. 4a and b, we find that the values of

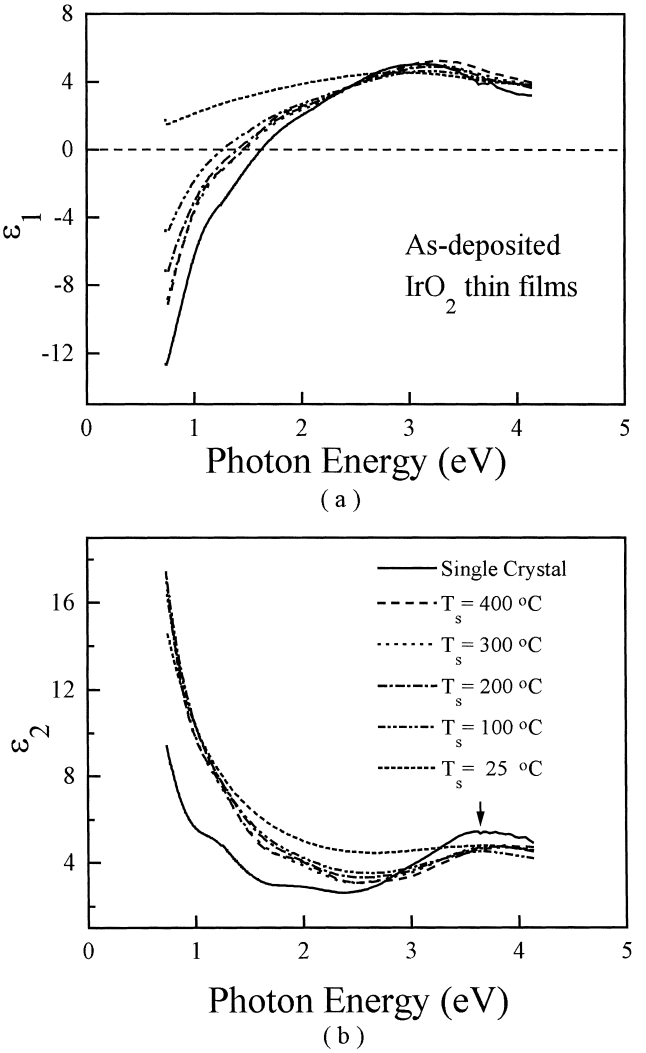


Fig. 4. The spectra of (a) the real part, $\epsilon_1$ and (b) imaginary part, $\epsilon_2$, of the dielectric function for the $IrO_2$ films.

$E_{th}$ fall in the range $1.27\pm0.02 < E_{th} < 1.46\pm0.02$ eV which is lower than the value of 1.7 eV for single crystal $IrO_2$ [16]. However, the $E_{th}$ for $RuO_2$ (figures not shown) is found to be $1.73\pm0.02$ eV which is close to $E_{th}=1.8$ eV for single crystal $RuO_2$ [16]. The effective mass of electrons for $RuO_2$ and $IrO_2$ is not available in literature at present. Therefore, the exact values of the plasma frequency for $IrO_2$ and $RuO_2$ cannot be estimated. In any case it will be well above the value of $\omega_{th}$.

The imaginary parts of the dielectric constants, $\epsilon_2(\omega)$ of the as-deposited $IrO_2$ films are shown in Fig. 4b. The structures at photon energies above ~3.0 eV are due to p→d interband transitions. The first p→d peak, indicated by an arrow, appears at around 3.65 eV. Similar features are also being reported for the single crystals of $IrO_2$ [16]. Our results of the $E_{th}$ for the interband transitions for $IrO_2$ film deposited at higher substrate temperature appears at $1.47\pm0.02$ eV and the first p→d peak at approximately $3.65\pm0.2$ eV. A similar study for the $RuO_2$ films show

$E_{th}=1.73\pm0.02$ eV and the first p→d peak at approximately 2.45±0.5 eV. These results agree reasonably well with the theoretical calculation of Xu et al. [17].

The first-order Raman spectra (RS) of the as-deposited $RuO_2$ and $IrO_2$ films are also undertaken and illustrated in Fig. 5a and b. For comparison purpose, the RS of the respective single crystals are also included in the figures. The three major peaks of the RS are designated as $E_g$, $B_{2g}$ and $A_{1g}$ modes. For single crystals $RuO_2$, we have $E_g$ at 528 $cm^{-1}$, $B_{2g}$ at 716 $cm^{-1}$ and $A_{1g}$ at 646 $cm^{-1}$ while that of single crystals $IrO_2$ have $E_g$, $B_{2g}$ and $A_{1g}$ modes at 561, 728 and 752 $cm^{-1}$, respectively. The red shift and linewidth of the three major features of the as-deposited $RuO_2$ films decreases monotonically with increasing substrate temperature. For $IrO_2$ films, the three major RS features show a slight blue shift. The linewidth of the three modes show a similar broadening behavior with decreasing substrate temperature. The increase in linewidth can be attributed to microcrystallinity and local disorder as exemplified by the X-ray diffraction measurements.

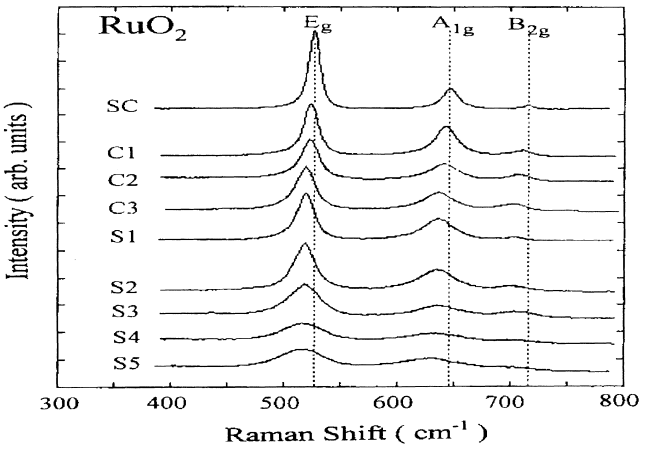


(a)

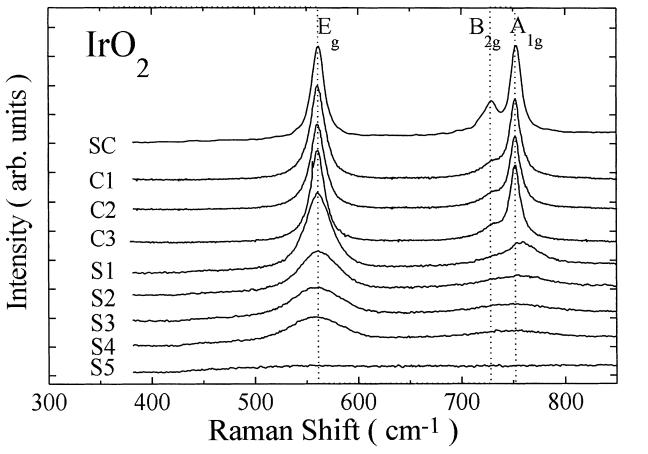


(b)

Fig. 5. The first-order Raman spectra of the $RuO_2$ and $IrO_2$ films on Si substrate prepared by MOCVD and reactive sputtering at different temperatures: (C1) MOCVD, $T_d=600$°C for $RuO_2$, $T_d=450$°C for $IrO_2$, (C2) MOCVD, $T_d=550$°C for $RuO_2$, $T_d=400$°C for $IrO_2$, (C3) MOCVD, $T_d=500$°C for $RuO_2$, $T_d=350$°C for $IrO_2$, (S1) sputtering, $T_d=400$°C, (S2) sputtering, $T_d=300$°C, (S3) sputtering, $T_d=200$°C, (S4) sputtering, $T_d=100$°C, (S5) sputtering, $T_d=25$°C. (SC) The spectra of the single-crystal $RuO_2$ and $IrO_2$ are included for comparison.

## 4. Summary

AFM, X-ray diffraction, electrical conductivity, ellipsometry and Raman scattering were used to characterize $RuO_2$ and $IrO_2$ films. The average grain sizes of the films increase as deposition temperature increases from 25 to 400°C. A grain boundary scattering model fits well with relation between the average grain size and electrical resistivity. The results of X-ray diffraction and Raman scattering measurements indicate the existence of microcrystallinity and local disorder with lower substrate temperature. The results of electrical and optical studies show a metallic character of the films deposited at higher temperature.

## Acknowledgements

The authors P.C.L. and Y.S.H. acknowledge the support of the National Science Council of the Republic of China under Project No. NSC89-2112-M-011-001 and K.K.T. acknowledges the support of the National Science Council of the Republic of China under Project No. NSC89-2112-M-019-002.

## References

[1] D.E. Stilwell, S.M. Park, J. Electrochem. Soc. 135 (1988) 2254.
[2] J. Rolewicz, C. Comninellis, E. Plattner, J. Hinden, Electrochem. Acta 33 (1988) 573.
[3] L. Krusin-Elbaum, Thin Solid Films 169 (1989) 17.
[4] L. Krusin-Elbaum, M. Wittmer, J. Electrochem. Soc. 135 (1988) 2610.
[5] A. Dziedzic, L. Golonka, J. Mater. Sci. 27 (1988) 3151.
[6] P.K. Khanna, S.K. Bhatnagar, M.L. Sicodia, J. Phys. D 22 (1988) 1766.
[7] Q.X. Jia, W.A. Anderson, Appl. Phys. Lett. 57 (1990) 304.
[8] M.L. Green, M.E. Gross, L.E. Papa, K.J. Schnoes, D. Brasen, J. Electrochem. Soc. 132 (1985) 67.
[9] Si, Desu, J. Mater. Res. 8 (1993) 2644.
[10] W.C. Dautremont-Smith, Displays 3 (1982) 67.
[11] K. Pasztor, A. Sekiguchi, N. Shimo, N. Kitamura, H. Masuhara, Sensors Actuators B 12 (1993) 225.
[12] X. Beebe, T.L. Rose, IEEE Trans. Biomed. Eng. 35 (1988) 494.
[13] T. Nakamura, Y. Nakao, A. Kamisawa, H. Takasu, Appl. Phys. Lett. 65 (1994) 1522.
[14] J.A. Woollam, P.G. Snyder, Mater. Sci. Eng. B 5 (1990) 279.
[15] A.F. Mayadas, M. Shatzkes, Phys. Rev. B 1 (1970) 1382.
[16] A.K. Goel, G. Skorinko, F.H. Pollak, Phys. Rev. B 24 (1981) 7342.
[17] J.H. Xu, T. Jarlborg, A.J. Freeman, Phys. Rev. B 40 (1989) 7939.